

Clumpy accretion onto black holes. I. Clumpy-ADAF structure and radiationJian-Min Wang^{1,2}, Cheng Cheng¹ and Yan-Rong Li¹**ABSTRACT**

In this paper, we investigate the dynamics of clumps embedded in and confined by the advection-dominated accretion flows (ADAF), in which collisions among the clumps are neglected. We start from the collisionless Boltzmann equation and assume that interaction between the clumps and the ADAF is responsible for transporting angular momentum of clumps outward. The inner edge of the clumpy-ADAF is set to be the tidal radius of the clumps. We consider strong and weak coupling cases, in which the averaged properties of clumps follow the ADAF dynamics and mainly determined by the black hole potential, respectively. We get the analytical solution of the dynamics of clumps for the two cases. The velocity dispersion of clumps is one magnitude higher than the ADAF for the strong coupling case. For the weak coupling case, we find that the mean radial velocity of clumps is linearly proportional to the coefficient of the drag force. We show that the tidally disrupted clumps would lead to accumulation of the debris to form a debris disk in the Shakura-Sunyaev regime. The entire hot ADAF will be efficiently cooled down by photons from the debris disk, giving rise to collapse of the ADAF and quench the clumpy accretion. Subsequently, evaporation of the collapsed ADAF drives resuscitate of a new clumpy-ADAF, resulting in an oscillation of the global clumpy-ADAF. Applications of the present model are briefly discussed to X-ray binaries, ionization nuclear emission regions (LINERs) and BL Lac objects.

Subject headings: accretion, accretion disks — black hole physics — hydrodynamics

1. Introduction

Accretion onto black holes is energy sources of various kinds of celestial high energy objects. Radiation hydrodynamics of the accretion has been established well and known as the standard accretion disk model (Shakura & Sunyaev 1973), the slim accretion disk (Abramowicz et al. 1988; Wang & Zhou 1999; Wang & Netzer 2003) and the advection-dominated accretion flows (ADAF) (Narayan & Yi 1994) in light of dimensionless accretion rates. These models are widely applied, however, it is not clear yet to what extent the known models represent a realistic description of the observed phenomena. Moreover, it should be noted that these models are based on the continuous fluid with radiation fields whereas the continuous disk is undergoing the thermal, viscosity or photon bubble instabilities. Clearly, the popular treatment of accretion disks as continuous fluid only holds as a zeroth-order approximation.

¹Key Laboratory for Particle Astrophysics, Institute of High Energy Physics, Chinese Academy of Sciences, 19B Yuquan Road, Beijing 100049, China

²National Astronomical Observatories of China, Chinese Academy of Sciences, 20A Datun Road, Beijing 100020, China

It arises from both theoretical and observational motivations that accretion onto black holes is clumpy rather than homogeneously continuous. Instabilities of the radiation-pressure dominated regions driven by thermal (Krolik 1998), magneto-rotational (Blaes & Socrates 2001; 2003) and photon bubble instabilities (Gammie 1998) create cold clumps in the disk, forming multi-phase medium around the black hole. As a general case of the simplest version, the two-phase disk-corona model has been suggested for many years (e.g. Galeev et al. 1979; Haardt & Maraschi 1993; Mayer & Pringle 2007). More generally, clumpy disk has been suggested for many years in light of the X-ray properties of X-ray binaries and active galactic nuclei (AGNs) (Guilbert & Rees 1988; Celotti et al. 1992; Collin-Souffrin et al. 1996; Kuncic et al. 1997; Celotti & Rees 1999; Yuan 2003; Lawrence 2011). Recently, low-luminosity AGNs (LLAGNs) presumed to be powered by the ADAF show components of big blue bumps like brighter AGNs and quasars (Maoz et al. 2007; but see Ho 2008 for a review), implying that there are cold matters in the hot flows. There are motivated arguments for the existence of clumpy disk both in AGNs (Kuncic et al. 1996; Kumar 1999) including low luminosity AGNs (Celotti & Rees 1999) and X-ray binaries (Malzac & Celotti 2002; Merloni et al. 2006). Similar to the LLAGNs, some X-ray binaries show broad $K\alpha$ components in the low states (Miller et al. 2006a,b; Tomsick et al. 2008; Reis et al. 2009, 2010). Most of previous efforts focus on the internal state of clumps and their reprocessing properties (Guilbert & Rees 1988; Celotti et al. 1992; Kuncic et al. 1996, 1997; Malzac & Celotti 2002; Merloni et al. 2006), however, dynamics of clumps in disks is insufficiently understood.

On the other hand, fates of the clumps embedded in accretion flows are poorly known when they are approaching the black hole. They would be tidally disrupted by the hole, of which the captured debris is eventually accreted onto the hole. Unlike the case of black hole capturing stars, the capture rates of clumps are so fast that the debris of disrupted clumps is accumulating with time. In this paper, we show that the emission from accretion of debris can efficiently cool the hot ADAF, and leads it to collapse, quenching the clumpy accretion. Being triggered through α -viscosity or evaporation, the collapsed ADAF (cADAF) revives as a new clumpy-ADAF. This is a cycle between clumpy-ADAF and the cADAF, which is driven by the clumps. Radiation from the clumpy-ADAF shows interesting temporal properties.

In this paper, we presume that clumpy structure in the ADAF has been formed through some mechanisms listed above in the ADAF, or produced in the transition regions between the ADAF and the Shakura-Sunyaev disk. Collisions among the clumps can be neglected in the present case. The goal of the present paper is to derive the dynamical equations of clumpy-ADAF and we fortunately obtain the analytical solution of the clump dynamics in the ADAF. We find that the captured clumps will accumulate from the tidally disruption radius, and the radiation from the debris disk efficiently cool the ADAF. The presence of the debris disk is driving the global clumpy-ADAF to oscillate. The model is briefly applied to X-ray binaries and low luminosity AGNs.

2. Assumptions and dynamical equations

2.1. Basic assumptions

Figure 1 shows the regimes of accretion disk models. We simply refer that slim disks have $\dot{m} \gtrsim 1$, standard model of Shakura-Sunyaev disk (SSD) works between $1 \gtrsim \dot{m} \gtrsim \dot{m}_2$, and accretion flows become advection-dominated when $\dot{m}_2 = \alpha_A^2 \approx 0.1\alpha_{0.3}^2$, where $\alpha_{0.3} = \alpha_A/0.3$ is the viscosity parameter of the ADAF, $\dot{m} = \dot{M}/\dot{M}_{\text{Edd}}$, \dot{M} is the accretion rates, $\dot{M}_{\text{Edd}} = L_{\text{Edd}}/\eta c^2 = 1.39 \times 10^{18} \eta_{0.1}^{-1} m_\bullet \text{ g s}^{-1}$, c is the light speed, $\eta_{0.1} = \eta/0.1$ is the radiative efficiency, $L_{\text{Edd}} = 1.25 \times 10^{38} m_\bullet \text{ erg s}^{-1}$ is the Eddington luminosity and $m_\bullet = M_\bullet/M_\odot$ is the black hole mass. When the accretion rates are low enough ($\dot{m} < \dot{m}_1$), flows become a

pure ADAF without clumps.

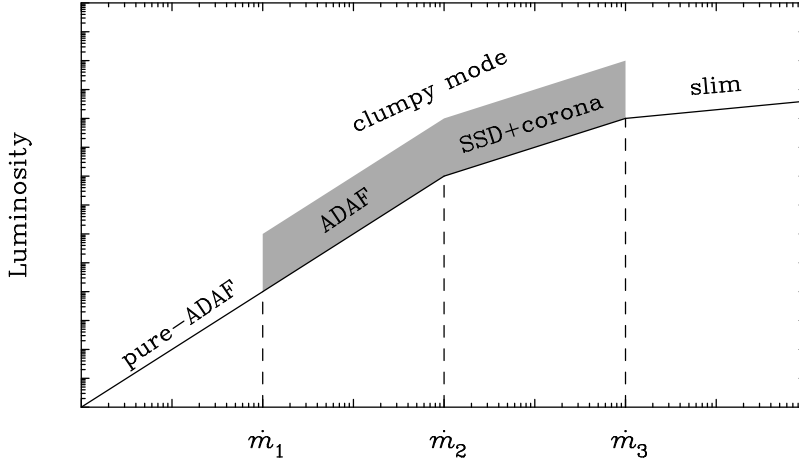


Fig. 1.— Accretion disk models in light of accretion rates. Accretion flows could develop clumpy structure indicated by the shaded regions. In the ADAF regimes, the radiated luminosity $L \propto \dot{m}^2$ whereas $L \propto \dot{m}$ in SSD regimes, and $L \propto \ln \dot{m}$ in the slim regime. It is not easy for a slim disk to develop a clumpy structure since its density is too high to develop thermal instability. On the other hand, slim disks ($\dot{m}_3 \sim 1$) only show weak features of hot corona above the disks, making the ionization parameter lower than that in SSD.

The critical accretion rate \dot{m}_1 can be roughly estimated from the ionization parameter, which is defined by $\Xi = L/4\pi R^2 cnk_B T$, where k_B is the Boltzmann constant, L is the radiated luminosity, R is the distance to the ionizing source, n and T is the density and temperature of the cold clumps. The self-similar solution of the simple ADAF model gives the thermal pressure $P_A = 1.7 \times 10^{16} \alpha^{-1} c_1^{-1} c_3^{1/2} m_\bullet^{-1} \dot{m} r^{-5/2}$ g cm $^{-1}$ s $^{-2}$, where $c_1 = (5+2\epsilon')g/3\alpha^2$, $c_2 = [2\epsilon'(5+2\epsilon')g/9\alpha^2]^{1/2}$, $c_3 = 2(5+2\epsilon')g/9\alpha^2$, $g = [1 + 18\alpha^2/(5+2\epsilon')^2]^{1/2} - 1$, $\epsilon' = (5/3 - \gamma)/f(\gamma - 1)$, γ is the adiabatic index and f is the advection-dominated factor (Narayan & Yi 1994). In this paper, we use $c_1 = 0.46$, $c_2 = 0.48$, $c_3 = 0.31$ for $\gamma = 1.4$, $f = 0.9$ unless we point out their specific values¹. The results in the present paper are not very sensitive to the values of γ and f . Using the scaling relation of ADAF, we have its bolometric luminosity $L_{\text{ADAF}} = 0.2(\dot{m}/\alpha)^2 L_{\text{Edd}}$ (Mahadevan 1997). Here we only use the single temperature of the ADAF model. The ionization parameter defined by $\Xi = L/4\pi R^2 c P_{\text{cl}}$ is used to describe the two-phase medium, where P_{cl} is the internal pressure of the clumps. We assume that the clumps hold a pressure balance with the ADAF ($P_{\text{cl}} = P_A$)², yielding the critical accretion rate as

$$\dot{m}_1 = 0.02 \alpha_{0.2} \Xi_{0.1}^{-1/2} r_{1000}^{-1/2}, \quad (1)$$

where $\Xi_{0.1} = \Xi/0.1$, $r_{1000} = R/1000R_{\text{Sch}}$, and $R_{\text{Sch}} = 2.95 \times 10^5 m_\bullet \text{cm}$ is the Schwarzschild radius. For cases with $10 > \Xi > 0.1$ (Krolik 1998), the ionized gas holds a two-phase state with two different temperatures and a pressure balance between the hot and cold medium. For gas with $\Xi > 10$, only hot phase exists whereas $\Xi < 0.1$ only cold phase. The timescale of the thermal instability is generally given by the line

¹In the self-similar ADAF model, $\gamma \in (4/3, 5/3)$ depends on the magnetic field density. Actually the numerical solutions of the ADAF avoid the $\gamma \neq 5/3$ case (Manmoto et al. 1997). For simplicity, we take an intermediate value of $\gamma = 1.4$ in calculations.

²The clumpy-Shakura-Sunyaev disk shows a different relation of the ionization parameter with the distance to the black hole. Since radiation pressure dominates in the inner regions, we have $\Xi \propto \dot{m} r^{-1/2}$, where the radiation pressure $P_{\text{rad}} \propto m_\bullet^{-1} r^{-3/2}$. Details of clumpy-SSD will be carried out in a forthcoming paper.

cooling process, which determines the formation timescale of clumps. With the cooling function (Böringer & Hensler 1989), we have $\Delta t_{\text{cl}} \sim n_e k_B T / n^2 \Lambda_{\text{line}} = 7 \times 10^5 n_6^{-1} T_6^{2.3}$ s for medium with one solar abundance. For an ADAF of $1M_\odot$ black hole, clumps could be produced at the interacting regions between the ADAF and the Shakura-Sunyaev disk, namely the evaporation region, where Δt_{cl} will be much shorter than that of the Keplerian rotation. Detailed analysis is needed to show the production of clumps through thermal instability. Figure 2 shows a cartoon of the clumpy-ADAF model.

We would like to point out that Kuncic et al. (1996) and Celotti & Rees (1999) present more arguments to support the general existence of cold clumps in the accretion disk. This lower limit (equation 1) for the clumpy-ADAF is only based on the thermal instability and is regarded as a characteristic critical value. The limit critical accretion rate could get lower if the magneto-rotational instability is included in the ADAF. Furthermore, we presume that the ADAF part of the global clumpy-ADAF can be described by the self-similar solution³. We do not consider the effects of ADAF-driven outflow on the clumps as known as advection-dominated inflow and outflows (ADIOS) (Blandford & Begelman 1999). However, it would be very interesting to postulate the situation which clumps could dynamically follow the outflows, forming clumpy outflows. ADIOS with clumps as a potential scenario will be considered in the future (the referee is acknowledged for this motivated point).

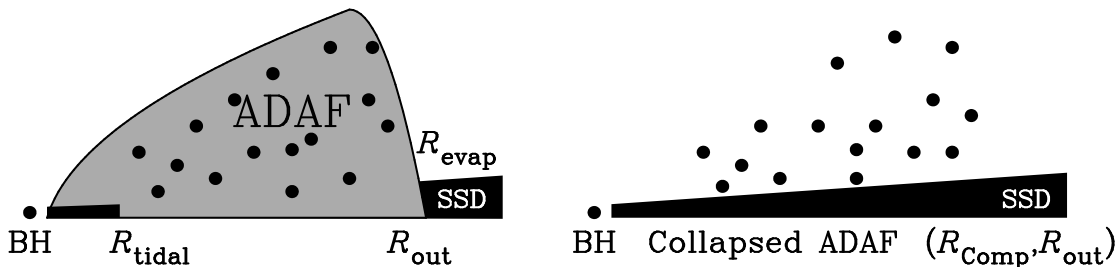


Fig. 2.— Cartoons of clumpy ADAF. *Left* panel: A tiny debris disk forms through accumulation of the tidally disrupted clumps by the black hole within the tidal radius (R_{tidal}). The disk can be accumulated up to the Shakura-Sunyaev regime. We set the tidal radius as the inner edge of the clumpy-ADAF, which is the outer radius of the debris disk. The radiation from the debris disk has strong feedback to the hot ADAF through Compton cooling, giving rise to a collapse of the ADAF and quenching the clumpy accretion. *Right* panel: The collapsed ADAF (cADAF). States of clumpy-ADAF transit to a cADAF through the debris disk, and versus through disk evaporation. This leads to a kind of quasi-periodical oscillation of the global accretion flows. The fates of clumps remain open, they totally either disappear or are orbiting around the black hole, or collide with the cADAF. See the text for details.

2.1.1. Clumps in the clumpy-ADAF

Existence of cold clumps can be simply justified by the thermal instability. Though detailed analysis is much beyond the scope of the present paper, we can use the simplified arguments to grasp the essentials here. The maximum size of clumps is determined by the crossing distance of sound wave within one Keplerian timescale, otherwise, the clumps are actually like a ring. This yields $R_{\text{cl}}^{\text{max}} \sim c_s t_{\text{Kep}} \approx 4.4 \times 10^{10} M_8 T_4^{1/2} r_{10}^{3/2}$ cm at radius R , where the sound speed $c_s = 10^6 T_4^{1/2}$ cm s⁻¹, $r_{10} = R/10R_{\text{Sch}}$ and $T_4 = T_{\text{cl}}/10^4$ K. On the other hand, the minimum size of clumps is determined by the thermal conduction, below which the

³The clumps will have dynamical feedback to the ADAF, but also the reprocessed emission could significantly cool the hot ADAF. We neglect these effects in this paper. Full treatments of the problem should couple clump equations with the ADAF.

clumps will be evaporated. Considering that line cooling dominates in the cold clumps (with a temperature of $\sim 10^4\text{K}$), the cooling rates $\Lambda_{\text{line}} \sim 8.0 \times 10^8 n_{14}^2 T_4^{-1.3} \text{ erg s}^{-1} \text{ cm}^{-3}$, where $n_{14} = n_{\text{cl}}/10^{14} \text{ cm}^{-3}$ (see the Figure 2 in Böhringer & Hensler 1989). For a Spitzer-like thermal conduction, the conduction rates are of $\mathcal{H} = \nabla \cdot (\kappa_{\text{S}} T^{2.5} \nabla T) \sim \kappa_{\text{S}} T^{3.5}/R_c^2 \approx 5.4 \times 10^8 T_{10}^{3.5}/R_{10}^2 \text{ erg s}^{-1} \text{ cm}^{-3}$ (Spitzer 1962). The necessary condition of $\mathcal{H} \leq \Lambda_{\text{line}}$ yields $R_{\text{cl}}^{\text{min}} \geq 0.82 \times 10^{10} T_{10}^{1.75} n_{14}^{-1} T_4^{0.65} \text{ cm}$. According to the pressure balance, the density of clumps is roughly of $n_{\text{cl}} = P_{\text{A}}/k_{\text{B}}T_{\text{cl}} = 2.1 \times 10^{16} M_8^{-1} \dot{m}_{-2} r_1^{-5/2} \text{ cm}^{-3}$. Generally, the size and mass of clumps could change with the distance to the black hole. For simplicity, we use the typical values of cloud mass and radius of clumps: $m_{\text{cl}} = 4\pi n_{\text{cl}} m_p R_{\text{cl}}^3/3 \approx 4 \times 10^{23} \text{g}$ and $R_{\text{cl}} \sim 10^{11} \text{cm}$ for a supermassive black hole with $10^8 M_{\odot}$, where m_p is the proton mass. It should be noted that the Thompson scattering depth of an individual cloud is of $\tau_{\text{es}} = n_{\text{cl}} R_{\text{cl}} \sigma_{\text{T}} = 6.65 n_{14} R_{11}$. On the other hand, the temperature of the clumps could keep a constant about 10^4K in light of efficient line cooling in the range of temperature $\sim 10^4\text{K}$ (Sutherland & Dopita 1993). Otherwise the clumps will be evaporated by the surrounding medium. We take an approximately constant temperature of clumps. Table 1 gives the values of typical clumps for stellar and supermassive black holes.

Turbulence excited by the magneto-rotational instability (MRI) is responsible for transfer of angular momentum of the ADAF, and interacts with clumps. However, the MRI-turbulence is not able to destroy the clumps in light of the energy argument. The energy density of the MRI-turbulence is about $\sim \alpha P_{\text{A}}$, of which P_{A} keeps balance with the thermal energy density of clumps (P_{cl}), we have $\alpha P_{\text{A}} < P_{\text{cl}}$ since $\alpha < 1$. The MRI-turbulence is only a small disturbance to the clumps. On the other hand, the clump size is much smaller than the typical length of the turbulence ($\alpha H_{\text{A}} \sim \alpha R$). Furthermore, the turbulent eddies with a comparable size with clumps have smaller kinetic energies according to the Kolmogorov's law as $E_k \propto k^{-5/3}$ (Landau & Lifschitz 1959), where E_k is the energy per unit wavelength number of turbulence, $k = 1/\lambda$ and λ is the length of turbulence. Therefore, the smaller eddies have an energy density $\ll \alpha P_{\text{A}}$, which is only a tiny fraction of clumps. It is thus a good approximation that clumps are simplified as particles, which can be described by the Boltzmann equation.

Total mass of cold clumps should be self-consistently determined by analysis of global thermal instability, but, instead, we use the mass ratio defined as $\mathfrak{M} = M_{\text{cl}}/M_{\text{ADAF}}$ (see Equation 33) as a free parameter, where M_{cl} is the total mass of clumps and M_{ADAF} is the total mass within the outer boundary of the ADAF, in the present model. The mass of cold clumps in ADAF is assumed to be comparable with the ADAF, otherwise, no significant effects can be created (see §4 for discussions).

When a black hole has relatively low accretion rates, the inner part of the Shakura-Sunyaev disk becomes optically thin, forming the so-called "hybrid" disk (Shapiro, Lightman & Eardley 1976; Wandel & Liang 1991). The ADAF as the inner region of the Shakura-Sunyaev disk with relatively low accretion rates then develops starting from this radius. Actually, the cold disk will be evaporated by the hot corona, forming the truncated disk, namely, forming an ADAF starting from the evaporation radius (Meyer & Meyer-Hofmeister 1994; Lu et al. 2004), where the evaporation rates are equal to the accretion rates. In this paper, we take the evaporation radius as the outer boundary radius of the clumpy-ADAF, $R_{\text{out}} = R_{\text{evap}} = 10^3 R_{\text{Sch}}$ (Liu & Taam 2009). The total mass of the ADAF can be simply estimated by $M_{\text{ADAF}} \approx 3.2 \times 10^{-2} M_{\odot} \dot{m}_{-2} M_8 r_{1000}^{3/2}$, where $\dot{m}_{-2} = \dot{m}/10^{-2}$ and $r_{1000} = R/1000 R_{\text{Sch}}$. Therefore, we have about $\mathcal{N}_{\text{tot}} = \mathfrak{M} M_{\text{ADAF}}/m_{\text{cl}} \sim 6 \times 10^9 \mathfrak{M} m_{22}^{-1}$ clumps, indicating that there are a plenty of small dense clumps in the ADAF. The mean distance of clumps is given by $\langle l \rangle = \mathcal{N}^{-1/3} \approx 1.0 R_{\text{Sch}}$ within $10^3 R_{\text{Sch}}$, the crossing timescale $\Delta t_{\text{cross}} = \langle l \rangle / \langle v_R^2 \rangle^{1/2} \approx 10^4 M_8 r^{-3/2} \text{s}$ for typical value $\langle v_R^2 \rangle^{1/2} \approx 0.1c$ (see Figure 4). Comparing with the Keplerian timescale $t_{\text{K}} \approx 10^3 M_8 r^{-3/2} \text{s}$, we find $\Delta t_{\text{cross}} > t_{\text{K}}$, indicating that collisions among clumps can be neglected. This guarantees the validity of the collisionless Boltzmann equation and its moment equations employed in this paper. This could

only work for clumpy-ADAF whereas collisions would be a key mechanism to transport angular momentum outward in a clumpy SSD.

2.1.2. Interaction between clumps and the ADAF

Clumps orbiting around the black hole deviate from the dynamics of the ADAF which is a radial flow with sub-Keplerian rotation. The motion of clumps is controlled by two factors: 1) black hole potential; 2) drag force arisen by the ADAF. Clumps gain or loss angular momentum by the interaction with the ADAF, leading to moving outward or inward, respectively, making the velocity dispersion with ADAF. Angular momentum of clumps is then carried away by the ADAF, in which α -viscosity is responsible for transfer ADAF's momentum outwards. In this paper, we use the drag force as $F_R = f_R(v_R - V_R)^2$ and $F_\phi = f_\phi(v_\phi - V_\phi)^2$, where V_R and V_ϕ are the radial and ϕ -velocity of the ADAF, respectively, f_R and f_ϕ are two coefficients (Mathews 1990; Cinzano et al. 1999). In principle, we should use velocities of the MRI-turbulence to estimate the drag force.

The drag force employed here is an approximation of the drag force in laminar flows. The drag force can be actually expressed by $F_{R,\phi} = f_{R,\phi} \left[v_{R,\phi} - (V_{R,\phi}^2 + \sigma_{R,\phi}^2)^{1/2} \right]^2 = f_{R,\phi} (v_{R,\phi} - \beta_{R,\phi} V_R)^2$, where $\beta_{R,\phi} = \left[1 + (\sigma_{R,\phi}/V_{R,\phi})^2 \right]^{1/2}$, $\sigma_{R,\phi}$ are the turbulent velocities, and the subscripts represent the R - and ϕ -directions, in turbulent flows. Since $V_{R,\phi}^2 \gtrsim c_s^2 = \alpha^{-1} \sigma_{R,\phi}^2$, we have $\beta_{R,\phi} \approx (1 + \alpha)^{1/2}$. Considering $\alpha < 1$, it would be a good approximation for us to use the laminar drag force ($\beta_{R,\phi} = 1$ in this paper).

The two coefficients f_R and f_ϕ can be approximately taken as constants, which independent of the ADAF density and the distance to the black hole. Clumps are undergoing contract along with spiraling-in. For a simple estimation, we have $n_{\text{cl}} R_{\text{cl}}^3 = n_{\text{cl},0} R_{\text{cl},0}^3$, where the subscript “0” indicates the initial value (i.e. at the outer boundary), if individual clumps keep their mass. With the help of the pressure balance with the ADAF, we have $R_{\text{cl}} = (P_A/P_{A,0})^{1/3} R_{\text{cl},0}$. Since the coefficients $f_{R,\phi} = n_A/(n_{\text{cl}} R_{\text{cl}}) = (T_{\text{cl}}/T_A) R_{\text{cl}}^{-1}$, we have $f_{R,\phi} = (P_A T_{\text{cl},0}/P_{A,0} T_{\text{cl}})^{1/3} T_{\text{cl}}/T_A R_{\text{cl},0}^{-1}$. Considering the contraction makes clumps a little bit hotter (efficiently being cooled by radiation), we assume $T_{\text{cl}} \propto R^{-\zeta}$ and $\zeta \ll 1$. We obtain $f_{R,\phi} \propto R^{(1-4\zeta)/6} R_{\text{cl},0}^{-1} \propto R^{1/30} R_{\text{cl},0}^{-1}$ if $\zeta = 0.2$. Without more details of ζ , we find the coefficients are not sensitive to the distance to the black holes. We therefore take the coefficients as two constants in this paper.

2.1.3. Inner edge of the clumpy-ADAF: tidal disruption

The orbiting clumps are suffering from the tidal disruption governed by the black hole. Self-gravitation of clumps is negligible, however, clumps still survive through keeping a pressure balance with the surroundings if the tidal distortion can be overcome by the thermal pressure of the ADAF. The tidal force reads $F_{\text{tidal}} \approx GM_\bullet m_{\text{cl}} R_{\text{cl}}/R^3$ for a cloud, where G is the gravitational constant and R is the distance to the hole. This tidal force is balanced by the thermal pressure of the ADAF, namely, $F_{\text{tidal}} = 4\pi P_A R_{\text{cl}}^2$. Since the clumps keep a pressure balance with the ADAF, we have $P_A = n_{\text{cl}} k_B T_{\text{cl}}$, where $n_{\text{cl}} = m_{\text{cl}}/\frac{4\pi}{3} R_{\text{cl}}^3 m_p$ is the mass density of the clumps. Tidal disruption happens when $F_{\text{tidal}} \geq 4\pi n_{\text{cl}} k_B T_{\text{cl}} R_{\text{cl}}^2$, yielding a natural limit of the

inner boundary radius

$$\mathcal{R}_{\text{in}} = \left(\frac{GM_{\bullet} m_p R_{\text{cl}}^2}{4\pi k_B T_{\text{cl}}} \right)^{1/3} \approx \begin{cases} 8.0 M_8^{-2/3} R_{11}^{2/3} T_4^{-1/3} R_{\text{Sch}}, \\ 8.0 M_1^{-2/3} R_3^{2/3} T_4^{-1/3} R_{\text{Sch}} \end{cases} \quad (2)$$

where $M_8 = M_{\bullet}/10^8 M_{\odot}$, $M_1 = M_{\bullet}/1 M_{\odot}$, $R_{11} = R_{\text{cl}}/10^{11} \text{cm}$, $R_3 = R_{\text{cl}}/10^3 \text{cm}$ and $T_4 = T_{\text{cl}}/10^4 \text{K}$. Here we set the temperature of clumps $T_{\text{cl}} = 10^4 \text{K}$. Within the tidal radius, clumps are destroyed to form a disk of debris or mixed with the ADAF. Some papers have studied the formation of accretion disk after tidal disruption of stars by supermassive black holes (e.g. Cannizzo et al. 1990; Strubbe & Quataert 2009). It is not the main goal of investigating the detailed processes of destroyed clumps to form an accretion disk, however, we focus on its influence on the ADAF in this paper. Following the popular treatment, we assume that the tidal radius is the location of disk after the orbit of captured debris has been circularized.

We would stress here that we use the parameters of clumps at the tidal radius throughout the whole ADAF though clumps are undergoing contraction. Collisions are neglected for the clumpy-ADAF, thus the contraction is not important in the present situation. We use the values of the parameters listed in Table 1 throughout the ADAF. Clumps could be different in size and density in outer parts of the ADAF. However, it will be very important for the standard disk with clumps. In such a case, clumps merger and fragment through collisions, depending on the size of the clumps. This is much beyond the scope of the present paper.

2.2. Collisionless Boltzmann equation

Defining the distribution function as $\mathcal{F} = \Delta\mathcal{N}/R\Delta R\Delta z\Delta\phi\Delta\mathbf{v}$, dynamics of clumps can be generally described by the Boltzmann equation. Unlike the normal stellar system, the clumps are moving in the SMBH potential, but also dragged by the ADAF. We start from the origin of collisionless Boltzmann equation (4-11) in Binney & Tremaine (1987)

$$\frac{\partial \mathcal{F}}{\partial t} + \sum_{\alpha=1}^6 \frac{\partial (\mathcal{F} \dot{w}_{\alpha})}{\partial w_{\alpha}} = 0, \quad (3)$$

where $(\mathbf{x}, \mathbf{v}) \equiv \mathbf{w}$ and $\dot{\mathbf{w}} \equiv (\dot{\mathbf{x}}, \dot{\mathbf{v}})$ are the coordinates in the phase space. Generally, for a stellar system, $\sum_{\alpha=1}^6 \partial \dot{w}_{\alpha} / \partial w_{\alpha} = 0$ holds. The Boltzmann equation reduces to $\partial \mathcal{F} / \partial t + \sum_{\alpha=1}^6 \dot{w}_{\alpha} \partial \mathcal{F} / \partial w_{\alpha} = 0$. The drag force on the clumps depends on the velocity, making the Boltzmann equation complicated. Considering the dependence of acceleration of clumps on their velocity, we re-cast the Boltzmann equation

$$\frac{\partial \mathcal{F}}{\partial t} + \sum_{i=1}^3 \left(v_i \frac{\partial \mathcal{F}}{\partial x_i} + \dot{v}_i \frac{\partial \mathcal{F}}{\partial v_i} + \mathcal{F} \frac{\partial \dot{v}_i}{\partial v_i} \right) = 0. \quad (4)$$

The third term in the bracket arises from the drag force, which disappears in a conservative system as described by Equation (4-13a) in Binney & Tremaine (1987). In a cylindrical coordinate, we have

$$\frac{\partial \mathcal{F}}{\partial t} + \dot{R} \frac{\partial \mathcal{F}}{\partial R} + \dot{\phi} \frac{\partial \mathcal{F}}{\partial \phi} + \dot{z} \frac{\partial \mathcal{F}}{\partial z} + \dot{v}_R \frac{\partial \mathcal{F}}{\partial v_R} + \dot{v}_{\phi} \frac{\partial \mathcal{F}}{\partial v_{\phi}} + \dot{v}_z \frac{\partial \mathcal{F}}{\partial v_z} + \mathcal{F} \left(\frac{\partial \dot{v}_R}{\partial v_R} + \frac{\partial \dot{v}_{\phi}}{\partial v_{\phi}} + \frac{\partial \dot{v}_z}{\partial v_z} \right) = 0, \quad (5)$$

where $\dot{R} = v_R$, $\dot{\phi} = v_{\phi}/R$ and $\dot{z} = v_z$. Motion equations of an individual cloud read

$$\dot{v}_R = -\frac{\partial \Phi}{\partial R} + \frac{v_{\phi}^2}{R} + F_R; \quad \dot{v}_{\phi} = -\frac{1}{R} \frac{\partial \Phi}{\partial \phi} - \frac{v_R v_{\phi}}{R} + F_{\phi}; \quad \dot{v}_z = -\frac{\partial \Phi}{\partial z}, \quad (6)$$

where $\Phi = GM_{\bullet}/(R^2 + z^2)^{1/2}$, $F_R = f_R(v_R - V_R)^2$ and $F_{\phi} = f_{\phi}(v_{\phi} - V_{\phi})^2$ are the drag forces per unit mass in the R - and ϕ -direction, respectively, V_R and V_{ϕ} are the radial and the rotational velocities of the ADAF. It should be noted that f_R and f_{ϕ} might be functions of cloud's parameter, such as, radius and density. Here we neglect the drag forces in z -direction. We have $\sum_{\alpha=1}^6 \partial \dot{w}_{\alpha} / \partial w_{\alpha} = 2f_{\phi}(v_{\phi} - V_{\phi}) + 2f_R(v_R - V_R)$ in the cylindric coordinate frame. Considering the ϕ -symmetry of the clumpy disk, we have

$$\frac{\partial \mathcal{F}}{\partial t} + v_R \frac{\partial \mathcal{F}}{\partial R} + v_z \frac{\partial \mathcal{F}}{\partial z} + \left(\frac{v_{\phi}^2}{R} - \frac{\partial \Phi}{\partial R} + F_R \right) \frac{\partial \mathcal{F}}{\partial v_R} + \left(F_{\phi} - \frac{v_R v_{\phi}}{R} \right) \frac{\partial \mathcal{F}}{\partial v_{\phi}} - \frac{\partial \Phi}{\partial z} \frac{\partial \mathcal{F}}{\partial v_z} +$$

$$2\mathcal{F} [f_{\phi}(v_{\phi} - V_{\phi}) + f_R(v_R - V_R)] = 0.$$

This is the final version of the Boltzmann equation used for dynamics of clumps in the following sections.

2.3. Moment equations

Following the popular treatment, we solve the moment equations of the Boltzmann equation. We define the averaged parameter in velocity-space as $\langle X \rangle = \mathcal{N}^{-1} \int X \mathcal{F} d\vec{v}$, where X is a parameter. Here we use $\mathcal{N} = \int \mathcal{N} d\vec{v}$. The zeroth-order moment equation can be obtained by integrating Equation (7)

$$\frac{\partial \mathcal{N}}{\partial t} + \frac{1}{R} \frac{\partial}{\partial R} (R \mathcal{N} \langle v_R \rangle) + \frac{\partial}{\partial z} (\mathcal{N} \langle v_z \rangle) = 0. \quad (8)$$

The first-order moment equations can be gained through multiplying Equation (7) by v_R , v_{ϕ} and v_z , respectively, and integrating the equations in velocity-space. The first moment equation is given by

$$\frac{\partial}{\partial t} (\mathcal{N} \langle v_R \rangle) + \frac{\partial}{\partial R} (\mathcal{N} \langle v_R^2 \rangle) + \frac{\partial}{\partial z} (\mathcal{N} \langle v_R v_z \rangle) + \mathcal{N} \left(\frac{\langle v_R^2 \rangle - \langle v_{\phi}^2 \rangle}{R} + \frac{\partial \Phi}{\partial R} \right) -$$

$$\mathcal{N} f_R (\langle v_R^2 \rangle - 2\langle v_R \rangle V_R + V_R^2) = 0,$$

the second

$$\frac{\partial}{\partial t} (\mathcal{N} \langle v_{\phi} \rangle) + \frac{1}{R^2} \frac{\partial}{\partial R} (R^2 \mathcal{N} \langle v_R v_{\phi} \rangle) + \frac{\partial}{\partial z} (\mathcal{N} \langle v_{\phi} v_z \rangle) - \mathcal{N} f_{\phi} (\langle v_{\phi}^2 \rangle - 2\langle v_{\phi} \rangle V_{\phi} + V_{\phi}^2) = 0, \quad (10)$$

and the third

$$\frac{\partial}{\partial t} (\mathcal{N} \langle v_z \rangle) + \frac{\partial}{\partial R} (\mathcal{N} \langle v_R v_z \rangle) + \frac{\partial}{\partial z} (\mathcal{N} \langle v_z^2 \rangle) + \frac{1}{R} \mathcal{N} \langle v_R v_z \rangle + \frac{\partial \Phi}{\partial z} \mathcal{N} = 0. \quad (11)$$

We will use these moment equations to discuss the dynamics of the clumpy disk.

For the ϕ - and z -direction symmetric clumpy ADAF, we have $\langle v_z \rangle = 0$, $\langle v_R v_z \rangle = 0$, $\langle v_{\phi} v_z \rangle = 0$ and re-cast the continuity equation as

$$\frac{1}{R} \frac{\partial}{\partial R} (R \mathcal{N} \langle v_R \rangle) = 0, \quad (12)$$

yielding the accretion rates of clumps as $\dot{M}_{\text{cl}} = -2\pi R H_{\text{A}} \mathcal{N} m_{\text{cl}} \langle v_R \rangle$. The first moment equation is reduced to

$$\frac{\partial}{\partial R} (\mathcal{N} \langle v_R^2 \rangle) + \mathcal{N} \left(\frac{\langle v_R^2 \rangle - \langle v_{\phi}^2 \rangle}{R} + \frac{\partial \Phi}{\partial R} \right) - \mathcal{N} f_R (\langle v_R^2 \rangle - 2\langle v_R \rangle V_R + V_R^2) = 0, \quad (13)$$

the second to

$$\frac{1}{R^2} \frac{\partial}{\partial R} (R^2 \mathcal{N} \langle v_R v_\phi \rangle) - \mathcal{N} f_\phi (\langle v_\phi^2 \rangle - 2 \langle v_\phi \rangle V_\phi + V_\phi^2) = 0, \quad (14)$$

and the third to

$$\frac{\partial}{\partial z} (\mathcal{N} \langle v_z^2 \rangle) + \frac{\partial \Phi}{\partial z} \mathcal{N} = 0. \quad (15)$$

Table 2 gives a summary of input and output parameters used in the present model. The above moment equations describe the dynamics of clumps, however, these are not close. We have to supplement additional physical considerations to proceed. We distinguish two classes of the dynamics in light of the strength of coupling between clumps and ADAF. When f_R and f_ϕ are large enough, the clumps are strongly coupled with ADAF so that the averaged dynamics of clumps follows the ADAF. For small f_R and f_ϕ , the clumps are weakly coupled with the ADAF, showing weak dependence on the ADAF.

3. Structure of clumpy disk

3.1. Strong-coupling case

In the strong-coupling case, the drag force is so strong that the averaged dynamics of the clumps follow the ADAF, namely, $\langle v_R \rangle = V_R$ and $\langle v_\phi \rangle = R\Omega_A$, where Ω_A is rotational velocity of the ADAF. So the factor f_ϕ should be larger than a critical one. This can be understood by the fact that both the specific angular momentum and the kinetic energy of clumps are about same with the gas of ADAF since they are born in the ADAF. Therefore, we have

$$\langle v_R \rangle = -2.12 \times 10^{10} \alpha c_1 r^{-1/2} \text{ cm s}^{-1}, \quad (16)$$

$$\langle v_\phi \rangle = 2.12 \times 10^{10} c_2 r^{-1/2} \text{ cm s}^{-1}, \quad (17)$$

$\langle v_R \rangle / \langle v_\phi \rangle = -\alpha c_1 / c_2$, and the height of the clumpy disk

$$H_A = 2.95 \times 10^5 c_3^{1/2} c_2^{-1} m r \text{ cm}. \quad (18)$$

From the continuity equation, we have

$$\mathcal{N} = -\frac{\dot{M}_{\text{cl}}}{4\pi R H_A \langle v_R \rangle m_{\text{cl}}}, \quad (19)$$

where \dot{M}_{cl} is the averaged accretion rates of clumps. From ϕ -motion equation, we have

$$\langle v_\phi^2 \rangle = \frac{1}{\mathcal{N} f_\phi} \frac{1}{R^2} \frac{d}{dR} (R^2 \mathcal{N} \langle v_R v_\phi \rangle) + 2 \langle v_\phi \rangle V_\phi - V_\phi^2 = -\frac{1}{2} \frac{\langle v_R v_\phi \rangle}{f_\phi R} + 2 \langle v_\phi \rangle V_\phi - V_\phi^2, \quad (20)$$

and $\langle v_\phi^2 \rangle / \langle v_\phi \rangle^2 = 1 + \alpha c_1 / 2 c_2 f_\phi R$. The radial motion is rewritten by

$$\frac{d \langle v_R^2 \rangle}{dR} + \frac{1}{R} \left(1 + \frac{d \ln \mathcal{N}}{d \ln R} - f_R R \right) \langle v_R^2 \rangle + \left(\left\langle \frac{\partial \Phi}{\partial R} \right\rangle - \frac{1}{R} \langle v_\phi^2 \rangle + f_R V_R^2 \right) = 0, \quad (21)$$

where

$$\left\langle \frac{\partial \Phi}{\partial R} \right\rangle = \frac{1}{H_A} \int_0^{H_A} \frac{\partial \Phi}{\partial R} dz \approx \frac{GM_\bullet}{R^2}.$$

Considering $d \ln \mathcal{N} / d \ln R = -3/2$ from Equation (19), we have

$$\frac{d\langle v_R^2 \rangle}{dR} - \frac{1}{R} \left(f_R R + \frac{1}{2} \right) \langle v_R^2 \rangle + R \left(\Omega_K^2 - \frac{\langle v_\phi^2 \rangle}{\langle v_\phi \rangle^2} \Omega_A^2 \right) + f_R V_R^2 = 0. \quad (22)$$

Clearly, the ϕ -motion has strong influence on the radial motion. Inserting $\langle v_\phi^2 \rangle$ and $\langle v_\phi \rangle$, we have

$$\frac{d\langle v_R^2 \rangle}{dR} - \frac{1}{R} \left(f_R R + \frac{1}{2} \right) \langle v_R^2 \rangle + \left[(1 - c_2^2) R - \frac{1}{2} \alpha c_1 c_2 f_\phi^{-1} \right] \Omega_K^2 + f_R V_R^2 = 0. \quad (23)$$

With the outer boundary condition of $\langle v_R^2 \rangle = V_{\text{out}}^2$ at $R = R_{\text{out}}$, we have the solution as

$$\langle v_R^2 \rangle = c^2 \left\{ \frac{1}{2} \left[\alpha^2 c_1^2 \Gamma_R \Lambda_{\frac{3}{2}}(\Gamma_R, r) + (1 - c_2^2) \Lambda_{\frac{5}{2}}(\Gamma_R, r) - \frac{\alpha c_1 c_2}{2 \Gamma_\phi} \Lambda_{\frac{7}{2}}(\Gamma_R, r) \right] + \frac{V_{\text{out}}^2}{c^2 r_{\text{out}}^{1/2}} e^{-\Gamma_R r_{\text{out}}} \right\} r^{1/2} e^{\Gamma_R r}, \quad (24)$$

where $\Gamma_R = f_R R_{\text{Sch}}$, $\Gamma_\phi = f_\phi R_{\text{Sch}}$ and the function

$$\Lambda_q(\Gamma_R, r) = \int_r^{r_{\text{out}}} x^{-q} e^{-\Gamma_R x} dx,$$

and $q = 3/2, 5/2, 7/2$. Figure 3 shows the properties of the function Λ_q . Equation (24) gives the solution of the clumps, which deviates from the ADAF.

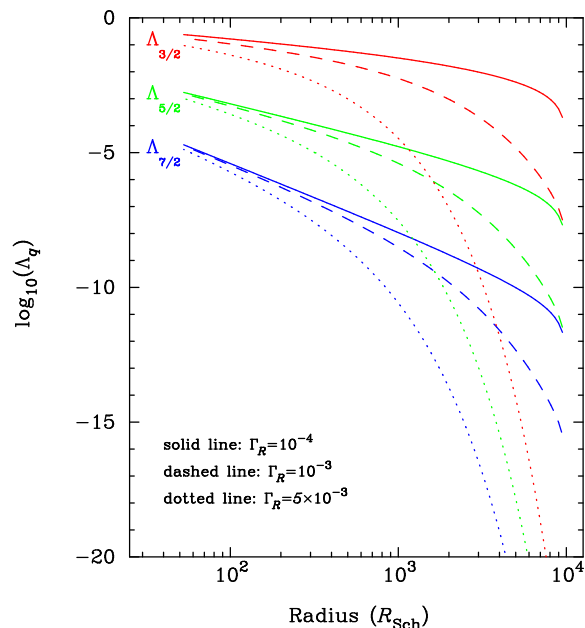


Fig. 3.— Properties of the function Λ_q . It is found that Λ_q is sensitive to the parameter Γ_R , but only at large radius. This property has strong influence on the radial velocity dispersion at large radii rather than that at small ones.

Physical meanings of each terms in Equation (24) can be examined under some extreme cases. Generally, clumps are controlled by two factors: 1) black hole potential; 2) ϕ - and R -direction drag forces. For a drag-free cloud, its orbit is determined purely by the black hole. When f_R tends to zero, namely $\Gamma_R = 0$, clumps are orbiting around black hole with ϕ -drag. Angular momentum of clumps is transferred by the

ADAF, in which the popular α -prescription works for outward transportation of the angular momentum of the ADAF, giving rise to fast spiral down to the black hole. In such a case, we have

$$\langle v_R^2 \rangle = \frac{1}{3}(1 - c_2^2) \frac{c^2}{r} \left[1 - \left(\frac{r}{r_{\text{out}}} \right)^{3/2} \right] - \frac{\alpha c_1 c_2}{20 \Gamma_\phi} \frac{c^2}{r^2} \left[1 - \left(\frac{r}{r_{\text{out}}} \right)^{5/2} \right] + \left(\frac{r}{r_{\text{out}}} \right)^{1/2} V_{\text{out}}^2. \quad (25)$$

The first term is the orbital motion around the black hole. The second term results in the accordance of cloud motion with the ADAF. The ϕ -drag decreases the velocity dispersion between the clumps and the ADAF. When the ϕ -drag is strong enough, we have the critical value

$$\Gamma_\phi^c \approx \frac{3\alpha c_1 c_2}{10(2 - 2c_2^2 - 3\alpha^2 c_1^2) r_{\text{in}}} \approx 8.7 \times 10^{-4} \alpha_{0.2} r_{10}^{-1}. \quad (26)$$

Here we neglect the terms of $(r_{\text{in}}/r_{\text{out}})$. When $\Gamma_\phi = \Gamma_\phi^c$, coupling with the ADAF is so strong that the velocity dispersion of clumps with the ADAF is zero at the tidal capture radius (R_{in}), namely, $\langle v_R^2 \rangle^{1/2} = V_{\text{in}}$ at $R = R_{\text{in}}$, where V_{in} is the radial velocity of the ADAF. So the strong coupling is referred to the case with $\Gamma_\phi > \Gamma_\phi^c$. Models with $\Gamma_\phi < \Gamma_\phi^c$ are the weak coupling and the strong coupling approximation does not work. We will discuss the case below.

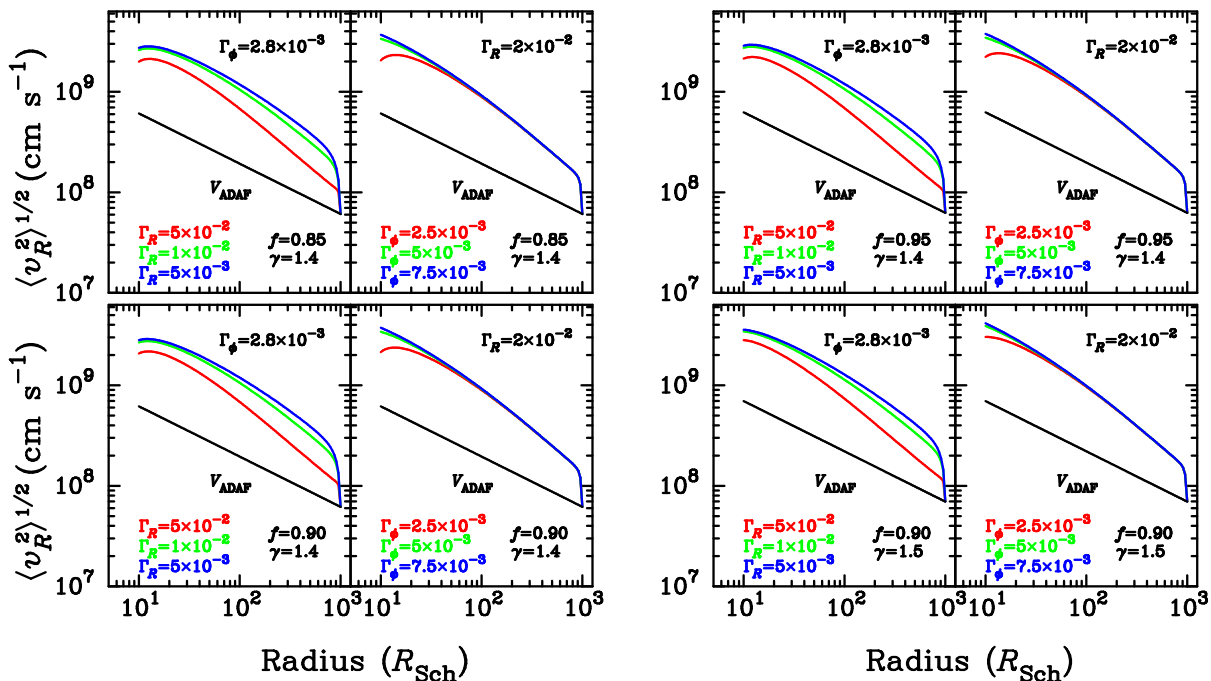


Fig. 4.— Solution of the clumpy-ADAF disk. The value of $\langle v_R^2 \rangle^{1/2}$ could be 10 times the radial velocity of ADAF. We note that the outer boundary does not significantly affect the properties of the inner part of clumpy-ADAF. The four panels show the dependence of the solution on the two index γ and factor f . It is found that the results are not sensitive to the two constants γ and f .

For an extremely strong-coupling, namely $\Gamma_\phi \rightarrow \infty$, clumps tend to have

$$\begin{aligned} \langle v_R^2 \rangle &= c^2 \left\{ \frac{1}{2} \left[\alpha^2 c_1^2 \Gamma_R \Lambda_{\frac{3}{2}}(\Gamma_R, r) + (1 - c_2^2) \Lambda_{\frac{5}{2}}(\Gamma_R, r) \right] + \frac{V_{\text{out}}^2}{c^2 r_{\text{out}}^{1/2}} e^{-\Gamma_R r_{\text{out}}} \right\} r^{1/2} e^{\Gamma_R r}, \\ &\approx \frac{1}{3} (1 - c_2^2) \frac{c^2}{r} \left[1 - \left(\frac{r}{r_{\text{out}}} \right)^{3/2} \right] + \left(\frac{r}{r_{\text{out}}} \right)^{1/2} V_{\text{out}}^2, \end{aligned} \quad (27)$$

namely, reaches its maximum. Here the first term with $\Lambda_{\frac{3}{2}}$ is always smaller than the others.

Figure 4 shows the solutions of the clumpy-disk for different parameters of the drag forces. For fixed Γ_ϕ case, it can be found that the radial drag strongly influences the velocity dispersion of clumps at large radii. On the other hand, for fixed Γ_R cases, $\langle v_R^2 \rangle$ is mainly determined by the Γ_ϕ and reaches its maximum as shown by Figure 4. We find the term involving $\Lambda_{3/2}$ is always smaller than the other two in Equation (24). This is due to radial velocity of the ADAF is smaller than the rotational, being represented by multiplying the factor α . Though the influence of the radial drag can be neglected, the present treatments are complete. The most important is that $\langle v_R^2 \rangle^{1/2} \sim 10 \langle v_R \rangle$ for the extremely strong coupling case from Figure 4. This means that the accretion rates of clumps are actually enhanced.

3.2. Weak-coupling case

When the birth of clumps are not very tightly linked with the ADAF in dynamics, the strong-coupling between clumps and the ADAF is relaxed. In such a case, of weak coupling with the ADAF, the assumptions of $\langle v_R \rangle = V_R$ and $\langle v_\phi \rangle = V_\phi$ do not work, and cloud dynamics resembles the stellar system. We introduce the velocity dispersions: $\sigma_R^2 = \langle v_R^2 \rangle - \langle v_R \rangle^2$, $\sigma_\phi^2 = \langle v_\phi^2 \rangle - \langle v_\phi \rangle^2$ and $\sigma_z^2 = \langle v_z^2 \rangle - \langle v_z \rangle^2$ to solve the moment equations. The moment equations should be closed up by physical considerations. Similar to stellar dynamics, we assume $\sigma_R^2 = k_R \sigma_z^2$ and $\sigma_\phi^2 = k_\phi \sigma_z^2$, where k_R and k_ϕ are two constants. Since clumps are produced by the ADAF in light of thermal instability and the velocity dispersion of clumps should be less than the sound speed of the ADAF, the vertical height of the clumpy disk does not exceed the ADAF height, we assume $H = H_A$. Employing $\langle v_z \rangle = 0$ and $\sigma_z^2 = \langle v_z^2 \rangle$, we have

$$\sigma_z = H_A \Omega_K, \quad (28)$$

After some algebraic manipulations, we re-cast Equation (17) and (18)

$$\left(\frac{\langle v_R \rangle^2 - \sigma_R^2}{\langle v_R \rangle} \right) \frac{d\langle v_R \rangle}{dR} - \frac{\langle v_\phi \rangle^2 + \sigma_\phi^2}{R} + \frac{d\sigma_R^2}{dR} + \left\langle \frac{\partial \Phi}{\partial R} \right\rangle = 0, \quad (29)$$

and

$$\langle v_R \rangle \frac{d\langle v_\phi \rangle}{dR} + \frac{\langle v_R \rangle}{R} \langle v_\phi \rangle - f_\phi \left[\sigma_\phi^2 + (\langle v_\phi \rangle - V_\phi)^2 \right] = 0, \quad (30)$$

where Equation (19) is used.

For a weak-coupling case, clumps are mainly orbiting around the black hole. The first term with $d\langle v_R \rangle/dR$, σ_ϕ^2/R and $d\sigma_R^2/dR$ are of the same order, but much smaller than the $\langle v_\phi \rangle^2/R$ and $\partial\Phi/\partial R$. So we have

$$\langle v_\phi \rangle \approx - \left\langle \frac{\partial \Phi}{\partial R} \right\rangle = V_K, \quad (31)$$

where V_K is the Keplerian velocity. Since $\langle v_\phi \rangle \approx V_K$, we have $\sigma_\phi \approx 0$ and $dv_\phi/dR \approx -v_\phi/2R$, Equations (30) yields

$$\langle v_R \rangle = \frac{2f_\phi R}{V_K} (V_K - V_\phi)^2 = 7.0 \times 10^4 \Gamma_{-5} r^{1/2} \text{ cm s}^{-1}, \quad (32)$$

where $\Gamma_{-5} = \Gamma_\phi/10^{-5}$. The mean velocity of clumps linearly proportional to the factor f_ϕ . The velocity dispersion $\langle v_R^2 \rangle = \sigma_R^2 + \langle v_R \rangle^2$ and $\langle v_\phi^2 \rangle = \sigma_\phi^2 + \langle v_\phi \rangle^2$ are known if k_R and k_ϕ are known, however, the present model is not able to determine k_R and k_ϕ in a self-consistent way. The two parameters should be constrained by observations. The weak coupling case does not have significant observable effects, we therefore remain it here.

As a brief summary, dynamics of clumps is very different from the ADAF whatever for strong and weak coupling cases between the clumps and the ADAF, but the dynamical properties of clumps depends on the ADAF. The prominent properties are: the velocity dispersion of clumps is one order higher or much smaller than the radial velocity of the ADAF in strong and weak-coupling cases, respectively. For the weak coupling, solutions of the clumps weakly coupled with the ADAF show that their properties are similar to stars in the black hole potential field. These properties of strong-coupling clumpy-ADAF determine variabilities of accretion disk of black holes.

Finally, we would like to point out the roles of magnetic fields discussed by Kuncic et al. (1996). For magnetized clumps, magnetic fields might be is in equipartition with the thermal pressure. The magnetic field plays a role in resisting the MRI-turbulence and makes the existence of clumps more persistent. Furthermore, magnetic fields lower the thermal conductivity (Spitzer 1962), and thus make clumps survive more robust. The real situations could be much complicated. Future numerical simulations would uncover more details of roles of magnetic fields in the clumpy-ADAF.

4. Radiation: observational appearances

Radiative properties of clumps in AGNs and X-ray binaries have been extensively studied by several authors (Kuncic et al. 1997; Celotti & Rees 1999; Malzac & Celotti 2002; Merloni et al. 2006). Much attention is given to the reprocessed emission from the clumps, emission lines are the main features. In such a case, profiles of emission lines could be broadened by the motions of clumps, and can be calculated through the method of Whittle & Saslaw (1986). The present paper investigates the case in which the debris of the tidally disrupted clumps is accumulating with time until a transient disk of the debris around the black hole forms. We show that the debris disk plays a key role in the radiation of the global accretion flows, in particular, feedback to the ADAF driven by the debris disk leads to a kind of quasi-periodical oscillation of the flows.

4.1. Capture rates of clumps

Considering the mass of clumps $\Delta M_{\text{cl}} = 4\pi R H_A \mathcal{N} m_c \Delta R$ within R to $R + \Delta R$ whereas the gas mass of the ADAF is $\Delta M_A = 4\pi R H_A \rho_A \Delta R$, we find the mass fraction of the clumps to the ADAF

$$\mathfrak{M} = \frac{\Delta M_{\text{cl}}}{\Delta M_A} = \frac{\dot{M}_{\text{cl}}}{\dot{M}_A}, \quad (33)$$

where \dot{M}_A is the accretion rates of the ADAF. In principle, the parameter \mathfrak{M} should be determined self-consistently by the model of cloud formation, but this is beyond the scope of the present paper. We treat it as a free parameter in the model.

The capture rates are given by the numbers of clumps which enter the tidal radius per unity time. Considering an interval time of Δt , we have the number of the captured clumps through the surface of the tidal radius $\Delta \mathcal{N} = 2\pi R_{\text{in}} H_{\text{in}} \mathcal{N}_{\text{in}} \langle v_R^2 \rangle^{1/2} \Delta t$, H_{in} and \mathcal{N}_{in} are the height of clumpy disk and clump number density at the tidal radius, respectively. Therefore we have the capture rates as $\dot{\mathcal{R}} = \lim_{\Delta t \rightarrow 0} (\Delta \mathcal{N} / \Delta t)$

$$\dot{\mathcal{R}} = \delta \mathfrak{M} \dot{m}_A \frac{\dot{M}_{\text{Edd}}}{m_{\text{cl}}} \approx \begin{cases} 1.4 \times 10^7 \eta_{0.1}^{-1} \delta_1 \mathfrak{M} \dot{m}_{-2} m_{10}^{-1} M_1 \text{ s}^{-1}, \\ 3.6 \times 10^9 \eta_{0.1}^{-1} \delta_1 \mathfrak{M} \dot{m}_{-2} m_{22}^{-1} M_8 \text{ month}^{-1}, \end{cases} \quad (34)$$

where $\delta = \langle v_R^2 \rangle^{1/2} / \langle v_R \rangle$, $\delta_1 = \delta / 10$, $\dot{m}_{-2} = \dot{M}_A / 10^{-2} \dot{M}_{\text{Edd}}$. We note that the capture rates are very high since $\langle v_R^2 \rangle^{1/2} \sim 10 \langle v_R \rangle$.

Since the capture timescale $\dot{\mathcal{R}}^{-1}$ is much smaller than the accretion of the debris onto black holes, the captured clumps are monotonically accumulating with time. For a single capture event, the tidally disrupted debris has complicated fates, which could resemble the capture stars (e.g. Rees 1988). However, it should be noted the difference of the present case from the captured star: the debris of disrupted clumps will interact with the ADAF. The circularization timescale could be of multiple Keplerian timescale of orbiting the black hole, leading to mix with local ADAF. On the other hand, after a series of captured clumps, a tiny disk of debris will be formed within the timescale of Δt_{cir} if the clumps take kinetic energy enough. The interaction among the debris of the captured clumps is very complicated, however, it is reasonable to assume that the timescale of forming the debris disk is of the order of Δt_{cir} .

4.2. Fates of captured clumps

Fates of disrupted clumps depend on both cloud's properties and the ADAF density. Similar to the case of the captured star, the debris of a disrupted cloud has a specific kinetic energy $\varepsilon \sim 3(GM_{\bullet}/R_P)(R_{\text{cl}}/R_P)$ for clumps approaching the black hole with a parabolic orbit, where R_P is the pericenter distance of the parabolic orbit (Lacy 1982; Evans & Kochanek 1989). After multiple cycles of the parabolic orbits, the gas flow will be circularized, forming a disk. The fallback timescale is given by

$$\Delta t_{\text{cir}}^{\text{min}} \approx \begin{cases} 0.7 M_1^{5/2} R_{P,3}^3 R_{\text{cl},3}^{-3/2} \text{ s}, \\ 2.2 M_8^{5/2} R_{P,3}^3 R_{\text{cl},11}^{-3/2} \text{ yr}, \end{cases} \quad (35)$$

where $R_{P,3} = R_P / 3R_{\text{Sch}}$ (e.g. Strubbe & Quataert 2009). Since the debris of clumps is embedded in the ADAF, the interaction between them is unavoidable. This makes it possible for the debris to mix with the ADAF when the interaction timescale is shorter than that of the circularization, otherwise the debris will form a disk of its own, called as a debris disk. This timescale is actually for the accumulation of debris disk ($\Delta t_{\text{acc}} \sim \Delta t_{\text{cir}}^{\text{min}}$).

4.2.1. Mixed with the ADAF

The swept mass rates of the debris is of $\dot{\mathcal{M}} \sim \pi R_{\text{cl}}^2 n_{\text{A}} \langle v_{\text{R}}^2 \rangle^{1/2} m_{\text{p}}$ and the lost energy rates are of $\dot{E}_{\text{K}} \sim \dot{\mathcal{M}} c_{\text{s}}^2$, where c_{s} is the sound speed of the ADAF. The timescale of dissipating the kinetic energy of the debris is given by

$$\Delta t_{\text{diss}} = \frac{E_{\text{K}}}{\dot{E}_{\text{K}}} \sim \frac{m_{\text{p}} \langle v_{\text{R}}^2 \rangle R_{\text{cl}}}{k_{\text{B}} T_{\text{cl}} \langle v_{\text{R}} \rangle} \approx \begin{cases} 1.2 \delta_1 \langle v_{\text{R}}^2 \rangle^{1/2} R_3 T_4^{-1} \text{ s}, \\ 3.8 \delta_1 \langle v_{\text{R}}^2 \rangle^{1/2} R_{11} T_4^{-1} \text{ yr}, \end{cases} \quad (36)$$

where $\langle v_{\text{R}}^2 \rangle^{1/2} = \langle v_{\text{R}}^2 \rangle^{1/2} / 10^8 \text{ cm s}^{-1}$, and the approximation of the pressure balance between clumps and the ADAF is used. We find that $\Delta t_{\text{diss}} \sim \Delta t_{\text{cir}}^{\text{min}}$ generally holds for small $\langle v_{\text{R}}^2 \rangle$ cases, but Δt_{diss} is significantly longer than $\Delta t_{\text{cir}}^{\text{min}}$ for large $\langle v_{\text{R}}^2 \rangle$ cases. This indicates formation of a debris disk, especially, for the very strong-coupling case.

When the debris is mixed with the ADAF, the density of the ADAF within the tidal radius will be enhanced generally, resulting in that cooling of the ADAF increases. Cooling enhancement by the mixture with the captured clumps could be moderately in this case. We will not pay much attention on this case, instead, on the case of forming a debris disk.

4.2.2. Formation of debris disk

As we shown below, capture of clumps is much faster than accretion onto black holes, yielding accumulation of debris around the hole. Since the clumps orbits are in the ADAF, the new disk of the accumulated debris will be inside the ADAF. Detailed formation of the debris disk could be very complicated (more than the case of the tidal disrupted stars, see Rees 1988; Strubbe et al. 2009). Here we assume that the formed disk holds the approximation of radiation-pressure dominated regions of the Shakura-Sunyaev disk since most of the gravitational energy will be released in this region. The accretion timescale driven by viscosity is given by $t_{\text{debris}} \approx R_{\text{debris}}^2 / \nu = \alpha^{-1} (H_{\text{debris}}/R)^{-2} t_{\text{K}}$, where $t_{\text{K}} = 1/\Omega_{\text{K}}$ is the Keplerian rotation timescale, R_{debris} and H_{debris} are the typical radius and scale height of the debris disk, respectively, and ν is the kinetic viscosity. Using the SSD solution, we have the accretion timescale

$$\Delta t_{\text{debris}} = \begin{cases} 1.56 \alpha_{0.2}^{-1} M_1 \dot{m}_{0.1}^{-2} r_{10}^{7/2} \text{ s}, \\ 4.96 \alpha_{0.2}^{-1} M_8 \dot{m}_{0.1}^{-2} r_{10}^{7/2} \text{ yr}, \end{cases} \quad (37)$$

where $r_{10} = R_{\text{in}}/10R_{\text{Sch}}$ and $\alpha_{0.2} = \alpha_{\text{SSD}}/0.2$. We find that $\dot{\mathcal{R}}^{-1} \ll \Delta t_{\text{debris}}$. Accumulation of the debris around the black hole follows the capture of clumps.

For an interval Δt , the accumulated mass of the captured clumps is $\Delta M_{\text{cl}} = m_{\text{cl}} \dot{\mathcal{R}} \Delta t$, where we neglect the swallowed clumps by the black hole during the accumulation. We have the accretion rates of the debris disk as $\dot{M}_{\text{debris}} = \Delta M_{\text{cl}} / \Delta t_{\text{debris}}$, and the dimensionless rate is

$$\dot{m}_{\text{debris}} = \delta \mathfrak{M} \dot{m}_{\text{A}} \left(\frac{\Delta t}{\Delta t_{\text{debris}}} \right) = 0.1 \delta_1 \mathfrak{M} \dot{m}_{-2} \Delta t_1, \quad (38)$$

where $\Delta t_1 = \Delta t / 1.0 \Delta t_{\text{debris}}$. We stress that the accretion rates of the debris disk is higher by one order than the undergoing ADAF arise from the fact of the radial velocity of clumps ($\delta \sim 10$) for the strong coupling

case. We would like to point out that the storage of the debris is undergoing through capturing the clumps since it carries too much kinetic energy to be directly accreted or mixed with the local ADAF.

It should be pointed out that the above estimation is based on the radiation pressure-dominated solution of SS73 model. The transition radius from gas to radiation pressure-dominated regions is $R_{\text{tr}}/R_{\text{Sch}} \approx 104.1 (\alpha m_{\bullet})^{2/21} (\dot{m}/\eta_{0.1})^{16/21}$. For $\dot{m} = 0.1$, we find that $R_{\text{tr}} \approx 18.0 (\alpha m_{\bullet})^{2/21} R_{\text{Sch}} > R_{\text{in}}$ holds generally. This means that the debris disk should be generally radiation pressure-dominated. For those debris disks dominated by gas pressure could still be in ADAF-regime until they reach in the SSD regimes. The present estimations are valid.

4.3. Feedback: collapse of ADAF?

4.3.1. Compton cooling as feedback to the ADAF

We show that a debris disk forms within $\Delta t \sim \Delta t_{\text{debris}}$ in the regime of the Shakura-Sunyaev model. The disk is radiating at a quite large luminosity, $L_{\text{debris}} = \eta \dot{M}_{\text{debris}} c^2 \sim 10^{45} \dot{m}_{0.1} M_8 \text{erg s}^{-1}$, where $\dot{m}_{0.1} = \dot{m}_{\text{debris}}/0.1$. Photons from the debris disk spanning from optics to UV for supermassive black holes and from UV to $\lesssim 1.0 \text{keV}$ for a few solar mass black holes provide extra sources to cool the hot electrons in the ADAF through Compton cooling with a timescale

$$\Delta t_{\text{Comp}} = \frac{n_e k_B T}{\Lambda_{\text{Comp}}} = \begin{cases} 54.1 M_1 \dot{m}_{0.1}^{-1} r_{1000}^2 \text{ ms} \\ 2.1 M_8 \dot{m}_{0.1}^{-1} r_{1000}^2 \text{ month,} \end{cases} \quad (39)$$

where $\Lambda_{\text{Comp}} = 2n_e k_B T \sigma_T F_{\text{debris}}/m_e c^2$ is the Compton cooling rates, the energy flux from the debris disk is $F_{\text{debris}} = L_{\text{debris}}/4\pi R^2$, $L_{\text{debris}} = \dot{m}_{\text{debris}} L_{\text{Edd}}$. Setting $t_{\text{Comp}} = \Delta t_{\text{debris}}$, we have the Compton radius, within which the ADAF is driven by the emergent photons from the debris disk to collapse through Compton cooling

$$R_{\text{Comp}} = 5447.0 \alpha_{0.2}^{-1/2} r_{10}^{7/4} \dot{m}_{0.1}^{-1/2} R_{\text{Sch}}. \quad (40)$$

We find that $R_{\text{Comp}} > (R_{\text{evap}}, R_{\text{out}})$, suggesting that the global ADAF will be cooled through Compton cooling. With such a strong feedback⁴, the ADAF collapses into geometrically thin disk since it has angular momentum. The collapse timescale is mainly controlled by the vertical gravity of the black hole. The collapsing velocity is given by $v_{\text{ff}} = H_{\text{Comp}} \Omega_K$, and the time scale is $\Delta t_{\text{collapse}} = \Omega_K^{-1} = 0.44 r_{1000}^{3/2} M_1 \text{ s} = 1.7 r_{1000}^{3/2} M_8 \text{ yr}$. This timescale is much shorter than the dynamical, shocks could be thus formed during the collapse and could heat the collapsed ADAF (hereafter cADAF). In this paper, we neglect this heating, which could be balanced by cooling of being condensed gas. The collapse stops until the cADAF reaches a new dynamical equilibrium of the Shakura-Sunyaev disk with a scale height of $H_{\text{cADAF}}/R = 4 \times 10^{-3} \dot{m}_{-2} r^{-1}$. In such a case clumps are then orbiting around the black holes without the ADAF-driven drag if they are bounded by magnetic field. It is also plausible for clumps collide with the cold disk and then are captured by the disk. They could undergo fast expansion and totally disappear since the pressure balance is broken.

⁴The steady ADAF is formed by the balance between gravity heating and cooling (free-free, synchrotron and inverse Compton scattering). Since the photon fluxes from the debris disk are much larger than the ADAF-generated energy flux ($L_{\text{debris}} \sim 0.1 L_{\text{Edd}}$ whereas gravity heating $L_G \lesssim 10^{-2} L_{\text{Edd}}$ in the ADAF itself), the ADAF is rapidly cooled through the Compton cooling without sufficient heating of released gravitational energy. Esin (1997) discussed the influence of non-local radiation on the ADAF, but it is different from the present case.

This feedback gives rise to quenching the clumpy accretions. The debris disk is playing as a switch in these processes.

4.3.2. Collapsed ADAF and revived clumpy-ADAF

The cADAF is undergoing two processes: 1) itself proceeds accretion onto black holes at a viscosity timescale; 2) it may be evaporated by hot corona from outer to inner regions. Though the formation of hot corona on the Shakura-Sunyaev disk remains open, we presume here that the two competing processes determine the post appearance of the cADAF. For the cADAF as an Shakura-Sunyaev disk, it is still radiation-pressure dominated and has a timescale of

$$\Delta t_{\text{cADAF}} = \begin{cases} 0.5 \alpha_{0.2}^{-1} M_1 \dot{m}_{0.1}^{-2} r_{1000}^{7/2} \text{ yr}, \\ 5.0 \times 10^7 \alpha_{0.2}^{-1} M_8 \dot{m}_{0.1}^{-2} r_{1000}^{7/2} \text{ yr}, \end{cases} \quad (41)$$

which is much longer than $\Delta t_{\text{collapse}}$. This makes the cADAF has the accretion rates of the previous ADAF, and radiate at $L_{\text{cADAF}} = \dot{m}_{\text{A}} L_{\text{Edd}} \approx 1.25 \times 10^{44} \eta_{0.1} \dot{m}_{-2} M_8 \text{ erg s}^{-1}$. The disk enters a relatively brighter state than the ADAF. The rising time scale is about $\Delta t_{\text{debris}} + \Delta t_{\text{Comp}}$ from the ADAF state. However, the fate of the cADAF is determined by the competition between the fueling black hole and evaporating the cADAF.

According to numerical calculations (Liu & Taam 2009), the evaporation timescale is given by

$$\Delta t_{\text{evap}} = \frac{M_{\text{cADAF}}}{\dot{M}_{\text{evap}}} \approx 1.45 r_{1000}^{3/2} \dot{m}_{-2} \dot{m}_{\text{evap},-2}^{-1} \text{ yr}, \quad (42)$$

where M_{cADAF} is the mass of the collapsed ADAF, which is roughly equal to total mass of the ADAF within R_{out} , and \dot{M}_{evap} is evaporation rates. The estimation simply follows from $\dot{M}_{\text{evap}} \sim 10^{-2} \dot{M}_{\text{Edd}}$, which depends on viscosity somehow. We would stress here that the evaporation timescale does not depend on black hole mass. Comparing Δt_{cADAF} with Δt_{evap} , we have $\Delta t_{\text{tran}} = \min(\Delta t_{\text{cADAF}}, \Delta t_{\text{evap}})$, indicating that evaporation could govern the post appearance of the cADAF in AGNs whereas viscosity of accretion does in X-ray binaries. We point out that accretion onto black holes in AGNs and X-ray binaries are different in this way. After the interval of Δt_{tran} , the clumpy-ADAF revives. A new cycle starts.

Figure 5 shows a cartoon of a cycle of the state transition in a black hole clumpy-ADAF. After the time Δt_{tran} , a new ADAF develops, and the object enters a low/hard state, switching on the clumpy accretion. Clumpy-ADAF is at low/hard state, but the cADAF corresponds to the high/soft state since it is Shakura-Sunyaev disk. State transition happens through the feedback of transient disk of the debris. The collapsed ADAF powering the high state will be brighter than the ADAF at the low/hard state. These processes correspond to transition of states in black hole X-ray binaries. For low luminosity AGNs, there could be a component as a big blue bump in some Low Ionization Nuclear Emission Regions (LINERs), especially in some LINERs with broad components of emission lines (Ho 2008). Furthermore, BL Lac objects have ADAF and some of them show light curves with quasi-periodical modulations, which could be explained by the present model. We stress that the transient disk plays a key role in feedback to the ADAF. The present model predicts a transition of accretion flows. There are two processes of shorter bursts: 1) emission from the debris disk; 2) cooling of the ADAF through the inverse Compton scattering. The first outburst proceeds to the second, especially, it is in soft band, and the second is a burst in hard X-ray band. Detailed

comparison with observations of X-ray binaries and AGNs would determine the size of the cADAF and the disk of the cloud’s debris.

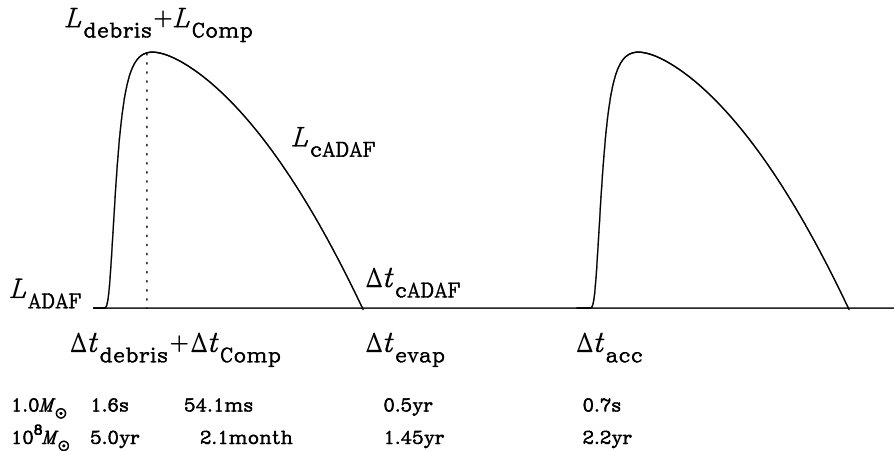


Fig. 5.— Characterized light curves of clumpy-ADAF. The long term averaged luminosity radiates at L_{ADAF} . The debris disk of tidally disrupted clumps is in Shakura-Sunyaev regime and efficiently radiates at a higher luminosity, and drives the hot ADAF to collapse into geometrically thin. The cADAF brings the accreting black hole to high/soft state with luminosity L_{cADAF} . The accretion timescale of the debris disk (Δt_{debris}) determines the size of the cADAF. Gas of the cADAF proceeds to being accreted onto black hole, in the meanwhile, evaporation develops a new ADAF with a timescale of Δt_{evap} governing the recurrence of the clumpy-ADAF in AGNs. After $\min(\Delta t_{\text{cADAF}}, \Delta t_{\text{evap}})$, clumpy accretion revives. This leads to a state transition in X-ray binaries, and sets up a quasi-periodical light curve in low luminosity AGNs. The quasi-period is given by Δt_{acc} and a burst duration by $\Delta t_{\text{debris}} + \Delta t_{\text{Comp}} + \Delta t_{\text{cADAF}}$. It should be noted that the timescales labeled are characterized ones and depends on some parameters. The timescales in the cartoon are not scaled.

4.4. Discussions

When an accretion flow has low enough rates, it turns to an ADAF by evaporation (Meyer & Meyer-Hofmeister 1994) and would become clumpy-ADAF with a critical accretion rate of $\dot{m} \gtrsim 0.02\alpha_{0.1}$ as shown in Figure 1. Clumps are finally disrupted by the tidal force of the black hole, forming a transient tiny disk. Liu et al. (2007) and Meyer-Hofmeister & Meyer (2011) suggest that an inner disk may be formed through condensations of ADAF if the accretion rates are in a reasonable range. In principle, this condensation model results from thermal instability, and is physically equivalent to the clumpy-ADAF model suggested in this paper. However, their model is different from the present in three aspects: 1) the tiny disk is persistent in Liu et al. (2007), but it is transient in the present model; 2) only two components (cold disk and ADAF) in Liu et al. (2007) and many clumps in the present model; 3) dynamics is different. As we shown below, the present model can conveniently explain more observations, besides the observed iron $K\alpha$ lines in AGNs (Meyer-Hofmeister & Meyer 2011), such as variabilities of X-ray binaries and radio-loud AGNs.

In the present model, we assume that clumps in the ADAF keep constant mass and radius before being tidally disrupted. Despite of these assumptions, it holds the main features of the clumpy accretion. We may relax some assumption in future studies. Here, we omit to discuss the weak coupling case of the clumpy-ADAF because it may give results without significant difference from the pure ADAF. On the other hand, if the accretion rates are in Shakura-Sunyaev disk regime, the dynamics of clumps could be changed into a phase driven by collisions among the clumps as well as the drag force in R - and ϕ -direction. Observations show that X-ray regions are partially covered by clumps (Gallo et al. 2004; Ballantyne et al. 2004; Ricci

et al. 2010; see a review of Turner & Miller 2009), implying clumps in the clumpy-SS disk will be much larger than the present. These contents will be discussed as the main goals of the second papers. We treat the outer boundary as the evaporation radius, where production of clumps is likely happening due to the thermal instability here. This should be issued in more detailed in a future paper.

Finally, numerical simulations of the dynamics and radiation of the clumpy-ADAF are worth doing to give more details like in dusty torus (Stalevski et al. 2011). We briefly discuss the radiation from the clumpy-ADAF in light of time scales of the undergoing processes. Collapse of the ADAF deals with energy release of gravitational energy in the vertical direction though this energy is smaller than the debris disk. The cADAF radiates is simplified as a Shakura-Sunyaev disk. This is valid when the collapse time scale is much shorter than the accretion time scale. Future numerical simulations will uncover the full processes of the collapse of the ADAF and radiation from the collapsed ADAF.

5. Observational tests and applications

The present clumpy-ADAF model only applies to those black holes which have a steady accretion rates in the ADAF regime with $\dot{m} \gtrsim 10^{-2}$ as shown by Equation (1). These accreting black holes could be used to test the predictions of the present model. We briefly illustrate to apply the present model to X-ray binaries and low luminosity AGNs to potentially explain the related phenomena, but detailed applications will be given in a separated paper.

5.1. Low luminosity AGNs: LINERs and BL Lacs

The active galactic nuclei well-known in the ADAF regime are LINERs (e.g. Ho 2008) and some BL Lac objects (e.g. Wang et al. 2002; 2003). Since the timescale of the transient disk is much longer than that in X-ray binaries, the component of the transient disk will be observed easily, but it varies at a time scale of years.

LINERs: evidence has been found for presence of significant component of the big blue bump observed in normal AGNs and quasars (Maoz et al. 2007). Pure reprocessing emission from clumps (their Figure 1 in Celotti & Rees 1999) is not enough to explain the component since the reprocessing emission gets a peak at $10^{14.5}\text{Hz}$. The transient disk originated from the captured clumps definitely contributes to its emission to $10^{14} \sim 10^{16}\text{Hz}$ in light of the Shakura-Sunyaev disk model. It is trivial to test this model in LINERs since the component of the debris disk has a variability with a time scale of years depending on the black hole masses and accretion rates of the ADAF. It should be noted that the selected LINERs to test the model should have relative higher accretion rates in the clumpy-ADAF regime rather than the pure ADAF mode. These LINERs have broad $\text{H}\alpha$ components, which are 25% LINERs (Ho 2008). They could have relatively higher accretion rates (Elitzur & Ho 2009) and thus contain clumps in the ADAF. These LINERs are expected to be monitored for variabilities to test the accretion processes.

BL Lac objects: they have lower accretion rates, likely in ADAF mode (Wang, Ho & Staubert 2002; 2003; Barth et al. 2003). It is expected that some of them could have clumpy-ADAF. The observed emission is overwhelmed by the boosted emission of relativistic jet, and the emission from the debris disk or cADAF is not directly visible. It is generally postulated that the ADAF will produce a relativistic jet somehow (e.g. Meier 2001), evidenced by X-ray binaries (e.g. Fender et al. 2010), for example, the radio galaxy

3C 120 (Marscher et al. 2002) and 3C 111 (Tombesi et al. 2011). As we have shown, the presence of the debris disk drives disappearance of the ADAF through efficient Compton cooling, and results in quenching jet formation. In such a case, thermal components (L_{debris} , L_{Comp} and L_{cADAF}) could be observed if the relativistic boosting jet emission less overwhelms this component. More interestingly, the model predicts a periodical presence of the clumpy-ADAF which could lead to a light curves with quasi-periodical modulation in light of intermittent production of jet in the clumpy-ADAF mode. Jet production quenches in the period of $\Delta t_{\text{debris}} + \Delta t_{\text{Comp}} + \Delta t_{\text{cADAF}}$. Radio light curves from the website⁵ with quasi-periodical modulations of a few years observed in some BL Lac objects and radio galaxies could be explained by the present model, for example, 0235+164, 3C 120, 0607-157, 0727-115, 1127-145, 1156+295, 1308+326, 1335-127, OT 129, BL Lac, 3C 446, 3C 345. These objects have supermassive black holes with mass of $10^8 \sim 10^9 M_{\odot}$ (Ghisellini & Celotti 2001; Barth et al. 2003; Wang et al. 2002, 2003) and Eddington ratios of $10^{-3} \sim 10^{-2}$ (Wang et al. 2003).

We note that some sources from this website, such as, 3C 273 are different from the sources above mentioned. These sources may have higher accretion rates than the ADAF in BL Lac types sources. This implies the necessity of clumpy standard accretion disk discussed in previous sections.

5.2. Black hole X-ray binaries: state transition

Extensive reviews of observed properties of black hole X-ray binaries and related theoretical explanations have been given by Remillard & McClintock (2006), McClintock & Remillard (2006), Done et al. (2007) and Belloni et al. (2011). Some black hole X-ray binaries show repeat transition from low to high states and versus. The present model predicts repeat transitions. From the long term light curves of 4U 1630-47, XTE J1650-500, XTE J1720-318, H 1743-322, SLX 1746-331, XTE J1859 and Cyg X-1, they usually have Eddington ratio of $L/L_{\text{Edd}} \sim 10^{-2}$, but show variabilities with two orders (Done et al. 2007). They show bursts with very steep rising and slow declining. For a simple estimation at hard state, the hard X-ray luminosity (at $\sim 100\text{keV}$) from the ADAF $L_{\text{HX}} \sim 2.5 \times 10^{35} (M_{\bullet}/M_{\odot}) \dot{m}_{-2} \text{erg s}^{-1}$ (Mahadevan 1997). Once formation of the debris disk, it is radiating at a luminosity of $L_{\text{SX}} \sim 1.3 \times 10^{37} (M_{\bullet}/M_{\odot}) (\dot{m}_{\text{debris}}/0.1)$ and the accreting black hole transit to at a high state with a around two order change ($L_{\text{HX}}/L_{\text{SX}} \sim 10^{-2}$). Detailed calculations of state transition and variability will be carried out in a forthcoming paper.

On the other hand, the presence of clumps in ADAF will increase the radiative efficiency of the ADAF, appearing the hard states with high luminosity (e.g. Figure 5 in the most recent review of Belloni et al. 2011). After the ADAF collapses, jet production quenches and the accretion flows then transit to high state. We note that the collapse of the ADAF will squeeze itself. The squeezed gas could be blown away by the radiation, yielding outflows. This happens during the transition of states, especially from low to high states. Detailed comparisons with observations will be given in a future paper.

6. Conclusions

We show that an ADAF becomes a clumpy ADAF composed of cold clumps arising from thermal instability when $\dot{m} \gtrsim 0.02\alpha_{0.2}r_{1000}^{-1/2}$. We set up the dynamics of clumpy accretion onto black holes, and focus on the clumpy ADAF in this paper. This model fills the regimes of the accretion mode from standard

⁵<http://www.astro.lsa.umich.edu/obs/radiotel/umrao.php>

disks to pure ADAF. Angular momentum of clumps is transported by the ADAF. We discuss the strong and weak coupling cases separately. The inner edge of the clumpy disk is set at the radius of tidal disruption. Analytical solutions of the clumpy ADAF are obtained for the two cases. For the strong coupling case, the root of the averaged radial velocity square can be one order higher than the ADAF, resulting in a fast capture of clumps through tidal force. For weak coupling case, clumps are mainly orbiting around the black hole. The tidally disrupted clumps are accumulating with time until an efficiently radiating disk forms. The ADAF is driven to collapse through the Compton cooling of photons from the disk. As a consequence, clumpy accretion stops then. This constitutes a quasi-periodical modulation. The model could explain the state transition in X-ray binaries as well as the broad $K\alpha$ lines in their low states. Thermal components observed in LINERs can be in principle explained by the model. Moreover, the observed light curves with quasi-periodical modulations in some BL Lac objects can be explained by the theoretical model as a result of quenching the ADAF through Compton cooling driven by the transient disk formed by the tidally captured clumps.

We study a simplified model that could capture much interesting – though not all of the detailed physics of the clumpy-ADAF. We would stress that the present model neglects collisions among clumps, but they are important for the clumpy Shakura-Sunyaev disk. Moreover, productions of cold clumps could happen in the entire regions where radiation pressure dominates and source function of clumps will appear in the Boltzmann equation. The complicated properties of variabilities are arisen by the collisions of clumps and will be studied in a forthcoming paper.

The authors are very grateful to the anonymous referee for useful reports, which clarify some points in the early version of the paper. We appreciate the stimulating discussions among the members of IHEP AGN group. S. Mineshige is thanked for motivated discussions as to the clumpy-ADAF during his stay of visiting IHEP. L. C. Ho and H.-Y. Zhou are acknowledged for useful comments and suggestions of LINER variabilities. The research is supported by NSFC-10733010, -10821061, and -11173023 and 973 project (2009CB824800).

REFERENCES

- Abramowicz, M. et al. 1988, *ApJ*, 332, 646
- Ballantyne, D. R., Turner, N. J. & Blaes, O. M. 2004, *ApJ*, 603, 436
- Barth, A., Ho, L. C. & Sargent, W. L. W. 2003, *ApJ*, 583, 134
- Barvainis, R. 1993, *ApJ*, 412, 513
- Barth, A. J., Ho, L. C. & Sargent, W. L. W. 2003, *ApJ*, 583, 134
- Belloni, T. M. et al. 2011, arXiv:1109.3388
- Binney, J. & Tremaine, S. 1987, *Galactic Dynamics*, Princeton University Press
- Blaes, O. & Socrates, A. 2001, *ApJ*, 553, 987
- Blaes, O. & Socrates, A. 2003, *ApJ*, 596, 509
- Blandford, R. D. & Begelman, M. C. 1999, *MNRAS*, 303, L1
- Böhringer, H. & Hensler, G. 1989, *A&A*, 215, 147

- Cannizzo, J., Lee, H.-M. & Goodman, J. 1990, *ApJ*, 351, 38
- Celotti, A., Fabian, A. & Rees, M. J. 1992, *MNRAS*, 255, 419
- Celotti, A. & Rees, M. J. 1999, *MNRAS*, 305, L41
- Cinzano, P. et al. 1999, *MNRAS*, 307, 433
- Chakrabarti, S. K. & Manickam, S. G. 2000, *ApJ*, 531, L41
- Chiang, C. Y., Done, C., Still, M. & Godet, O. 2010, *MNRAS*, 403, 1102
- Collin-Souffrin, S., Czerny, B., Dumont, A.-M. & Zycki, P. T., 1996, *A&A*, 314, 393
- Done, C., Gierlinski, M. & Kubota, A. 2007, *A&A Rev*, 15, 1
- Elitzur, M. & Ho, L. C. 2009, *ApJ*, 701, L91
- Evans, C. & Kochanek, C. 1989, *ApJ*, 346, L13
- Esin, A. 1997, *ApJ*, 482, 400
- Fender, R. P., Gallo, E. & Russell, D. 2010, *MNRAS*, 406, 1425
- Field, G. B. 1965, *ApJ*, 142, 531
- Haardt, F. & Maraschi, L. 1993, *ApJ*, 413, 507
- Ho, L. C. 2008, *ARA&A*, 46, 475
- Galeev, et al. 1979, *ApJ*, 229, 318
- Gallo, L. et al. 2004, *MNRAS*, 353, 1064
- Gammie, C. 1998, *MNRAS*, 297, 929
- Ghisellini, G. & Celotti, A. 2001, *A&A*, 379, L1
- Krolik, J. 1998, *ApJ*, 498, L13
- Kumar, P. 1999, *ApJ*, 519, 599
- Kuncic, Z., Blackman, E. G. & Rees, M. J. 1996, *MNRAS*, 283, 1322
- Kuncic, Z., Celotti, A. & Rees, M. J. 1997, *MNRAS*, 284, 717
- Lacy, J. H., Townes, C. H. & Hollenbach, D. J. 1982, *ApJ*, 262, 120
- Landau, L. D. & Lifschitz, E. M. 1959, *Fluid Mechanics*.
- Liu, B. F., Taam, R. E., Meyer-Hofmeister, E. & Meyer, F. 2007, *ApJ*, 671, 695
- Liu, B. F. & Taam, R. 2009, *ApJ*, 707, 233
- Lawrence, A. 2011, [arXiv:1110.0854](https://arxiv.org/abs/1110.0854)
- Lu, J.-F., Lin, Y.-Q. & Gu, W.-M. et al. 2004, *ApJ*, 602, L37

- Mahadevan, R. 1997, ApJ, 477, 585
- Malzac, J. & Celotti, A. 2002, MNRAS, 335, 23
- Maoz, D. et al. 2007, MNRAS, 377, 1696
- Manmoto, T., Mineshige, S. & Kusunose, M. 1997, ApJ, 489, 791
- Marscher, A. et al. 2002, Nature, 417, 625
- Mathews, W. G. 1990, ApJ, 354, 468
- Mayer, M. & Pringle, J. E. 2007, MNRAS, 376, 435
- McClintock, J. E. & Remillard, R. A. 2006, In *Compact stellar X-ray Sources*, ed. W. H. G. Lewin, M. van der Klis, pp. 157-214. Cambridge: Cambridge University Press (astro-ph/0306213)
- Meier, D. 2001, ApJ, 548, L9
- Merloni, A., Malzac, J., Fabian, A. C. & Ross, R. R. 2006, MNRAS, 370, 1699
- Meyer, F. & Meyer-Hofmeister, E. 1994, A&A, 288, 175
- Meyer-Hofmeister, E. & Meyer, F. 2011, A&A, 527, 127
- Miller, J. M., Homan, J. & Miniutti, G. 2006a, ApJ, 652, L113
- Miller, J. M., Homan, J. et al. 2006b, ApJ, 653, 525
- Narayan, R. & Yi, I. 1994, ApJ, 428, L13
- Rees, M. J. 1988, Nature, 333, 523
- Reis, R. C., Miller, J. M. & Fabian, A. C. 2009, MNRAS, 395, L52
- Reis, R. C., Fabian, A. C. & Miller, J. M. 2010, MNRAS, 402, 836
- Remillard, R. A. & McClintock, J. E. 2006, ARA&A, 44, 49
- Ricci, C., Beckmann, V., Audard, M. & Courvoisier, T. J.-L., 2010, A&A, 518, 47
- Shakura, N. I. & Sunyaev, R. 1973, A&A, 24, 337
- Shapiro, S. L., Lightman, A. P. & Eardley, D. M. 1976, ApJ, 204, 187
- Spitzer, L. 1962, Physics of fully ionized gas (New York: Interscience), p87-88
- Stalevski, M. et al. 2011, MNRAS, in press, arXiv:1109.1286
- Strubbe, L. E. & Quataert, E. 2009, MNRAS, 400, 2070
- Sutherland, R. S. & Dopita, M. A. 1993, ApJS, 88, 253
- Tombesi, F. et al. 2011, MNRAS, (arXiv:1108.6095)
- Tomsick, J. A. et al. 2008, ApJ, 680, 593

- Turner, T. J. & Miller, J. 2009, *A&A Rev.*, 17, 47
- Wandel, A. & Liang, E. P. 1991, *ApJ*, 380, 84
- Wang, J.-M., Ho, L. C. & Staubert, R. 2003, *A&A*, 409, 887
- Wang, J.-M. & Netzer, H. 2003, *A&A*, 398, 927
- Wang, J.-M., Staubert, R. & Ho, L. C. 2002, *ApJ*, 579, 554
- Wang, J.-M. & Zhou, Y.-Y. 1999, *ApJ*, 516, 420
- Whittle, M. & Saslaw, W. C. 1986, *ApJ*, 310, 104
- Yuan, F. 2003, *ApJ*, 594, L99

Table 1. VALUES OF COLD CLOUD PARAMETERS IN THE CLUMPY-DISK

stellar mass BH			supermassive BH		
R_{cl} (cm)	m_{cl} (g)	n_{cl} (cm^{-3})	R_{cl} (cm)	m_{cl} (g)	n_{cl} (cm^{-3})
10^3	4×10^{10}	10^{23}	10^{11}	4×10^{23}	10^{14}

Table 2. PARAMETERS OF THE PRESENT MODEL

Parameter	Physical meanings
input parameters	
M_{\bullet}	black hole mass
\dot{M}_{A}	accretion rates of the continuous flow
\dot{M}_{cl}	averaged accretion rates of the clumps
m_{cl}	averaged mass of individual clumps
R_{in}	the tidal radius as the inner radius of the clumpy-ADAF
R_{out}	outer radius of the clumpy-ADAF
R_{cl}	averaged radius of individual clumps
n_{cl}	hydrogen number density of clumps
\mathfrak{M}	ratio of the ADAF and clumps mass ($= \dot{M}_{\text{cl}}/\dot{M}_{\text{A}}$)
α	viscosity parameter of the ADAF
Γ_R	coefficient of R -direction drag force
Γ_{ϕ}	coefficient of ϕ -direction drag force
output parameters	
\mathcal{N}	number density of the clumps
$\langle v_R \rangle$	averaged R -direction velocity
$\langle v_R^2 \rangle$	averaged of v_R^2
$\langle v_{\phi} \rangle$	averaged ϕ -direction velocity
$\langle v_{\phi}^2 \rangle$	averaged values of v_{ϕ}^2
\mathcal{R}	capture rates of clumps

A. Energy equation of clumps: the second moment equation

Section 2.2 gives the zeroth- and the first-order moment equations of the clumps. We use the strong-coupling condition to close up the moment equations. Energy equation of clumps can be obtained from the second-order moment equation, which can be obtained by multiplying and integrating $v_R v_\phi d\vec{v}$:

$$\begin{aligned} \frac{\partial}{\partial R} (\mathcal{N} \langle v_R^2 v_\phi \rangle) + \frac{\partial}{\partial z} (\mathcal{N} \langle v_R v_\phi v_z \rangle) - \frac{\mathcal{N} \langle v_\phi^3 \rangle}{R} + \mathcal{N} \langle v_\phi \rangle \frac{\partial \Phi}{\partial R} + \frac{2\mathcal{N} \langle v_R^2 v_\phi \rangle}{R} - f_R \mathcal{N} \langle v_\phi v_R^2 \rangle \\ + 2f_R \mathcal{N} V_R \langle v_R v_\phi \rangle - f_R \mathcal{N} V_R^2 \langle v_\phi \rangle - f_\phi \mathcal{N} \langle v_R v_\phi^2 \rangle + 2f_\phi \mathcal{N} V_\phi \langle v_R v_\phi \rangle - f_\phi \mathcal{N} V_\phi^2 \langle v_R \rangle = 0. \end{aligned} \quad (\text{A1})$$

For the ϕ - and z -direction symmetric clumpy ADAF, we have the following relations

$$\langle v_R^2 (v_\phi - \langle v_\phi \rangle) \rangle = \langle v_R^2 v_\phi \rangle - \langle v_R^2 \rangle \langle v_\phi \rangle = 0, \quad (\text{A2})$$

$$\langle v_R v_z (v_\phi - \langle v_\phi \rangle) \rangle = \langle v_R v_z v_\phi \rangle - \langle v_R v_z \rangle \langle v_\phi \rangle = 0, \quad (\text{A3})$$

$$\langle (v_\phi - \langle v_\phi \rangle)^3 \rangle = \langle v_\phi^3 \rangle - 3\langle v_\phi^2 \rangle \langle v_\phi \rangle + 2\langle v_\phi \rangle^3 = 0, \quad (\text{A4})$$

$$\langle v_R v_z \rangle = 0, \quad (\text{A5})$$

and subtract v_ϕ times the moment equation (9), then we obtain the energy equation

$$\frac{\partial \ln (\langle v_\phi \rangle R)}{\partial \ln R} \frac{\mathcal{N} \langle v_R^2 \rangle \langle v_\phi \rangle}{R} - \frac{2\mathcal{N} \langle v_\phi \rangle \sigma_\phi^2}{R} - f_\phi \mathcal{N} \langle v_R v_\phi^2 \rangle + 2f_\phi \mathcal{N} V_\phi \langle v_R v_\phi \rangle - f_\phi \mathcal{N} V_\phi^2 \langle v_R \rangle = 0, \quad (\text{A6})$$

where

$$\sigma_\phi^2 = \langle v_\phi^2 \rangle - \langle v_\phi \rangle^2. \quad (\text{A7})$$

When $f_\phi = 0$, equation (A6) reduces to equation (4-51) in Binney & Tremaine (1987). The energy equation introduces a new unknown parameter $\langle v_R v_\phi^2 \rangle$. In order to close up the moment equations, observational relations should be employed, such as, ratios of velocity dispersion. This can be done as in galactic dynamics, but it is very difficult for the present case. We thus take the strong coupling approximations.